ELSEVIER

Engineering Structures 24 (2002) 281–293

ENGINEERING STRUCTURES

www.elsevier.com/locate/engstruct

Investigation of semi-active control for seismic protection of elevated highway bridges

Baris Erkus *, Masato Abé, Yozo Fujino

Department of Civil Engineering, The University of Tokyo, Hongo 7-3-1, Bunkyo-ku, Tokyo 113-8656, Japan

Abstract

The applicability of semi-active control for seismic protection of elevated highway bridges is investigated through comparison with active and passive systems. A bridge pier–bearing–deck structure is modeled as a linear two-degree-of-freedom system and three design goals are studied: reduction of pier response, reduction of bearing response and reduction of both responses. The passive system is assumed to have a high-damping rubber bearing and linear quadratic regulator (LQR) control is used for the active system. Normalized peak displacements are used to optimize bearing damping and LQR parameters. LQR-based clipped optimal control is used to command a magneto-rheological (MR) damper in semi-active control, where the MR damper is designed according to deterministic analysis of the active system. Numerical simulations show that semi-active control can reach active control performance if the design goal is to reduce bearing response, while it shows similar behavior to the passive system if the design goal is to reduce pier response. All strategies showed similar performance for the reduction of both responses.

Keywords: Highway bridges; Optimal design; Semi-active control; Magneto-rheological damper

1. Introduction

During the past decades there has been extensive research on structural control concepts and technologies, which has led to successful applications to civil engineering structures. Each control strategy has its merits and disadvantages depending on the nature of the problem, purpose, structure, devices used, etc. For example, rubber bearings became very popular for seismic isolation of bridges and active systems were utilized in high-rise buildings to reduce wind-induced vibration.

Semi-active control for seismic protection of structures received special attention after the development of a new device called the magneto-rheological (MR) damper. Experimental and numerical studies show that semi-active control with MR dampers increases the seismic performance of a structure considerably, and in some cases it surpasses the active performance [1,2]. However, these studies were mainly on frame-type structures. Although some experimental and numerical studies of semi-active control of highway bridges are reported [3,4], control of bridges using MR dampers has not been reported yet. These new strategies should be investigated for highway bridges to increase seismic performance.

The starting point of the investigation of new semi-active strategies for bridges is modeling of the structural system. A typical elevated highway bridge consists of decks, bearings and piers. The easiest, yet most realistic model of a bridge deck–bearing–pier system for numerical analysis is to model the deck as a rigid body and the piers as single-degree-of-freedom (SDOF) systems where the whole mass is lumped at the top of the pier. A model with two degrees-of-freedom (DOFs) may be used for the passive system with rubber bearings if the girder is continuous with one pier and one bearing or several piers and bearings with same characteristics, as shown in Fig. 1(a), and piers are excited by the same ground motion. This model can also be used for active and semi-active systems if the control devices are attached to the system as shown in Fig. 1(b) and commanded by the same control law. Although it is simple, a two-DOF system is quite informative for an initial study and is used in this paper.

Based on the two-DOF model, passive, active and

* Corresponding author. Tel.: +81-3-5841-6096; fax: +81-3-5841-7454.

E-mail address: berkus@bridge.t.u-tokyo.ac.jp (B. Erkus).

0141-0296/02/$ - see front matter
PII: S0141-0296(01)00095-5

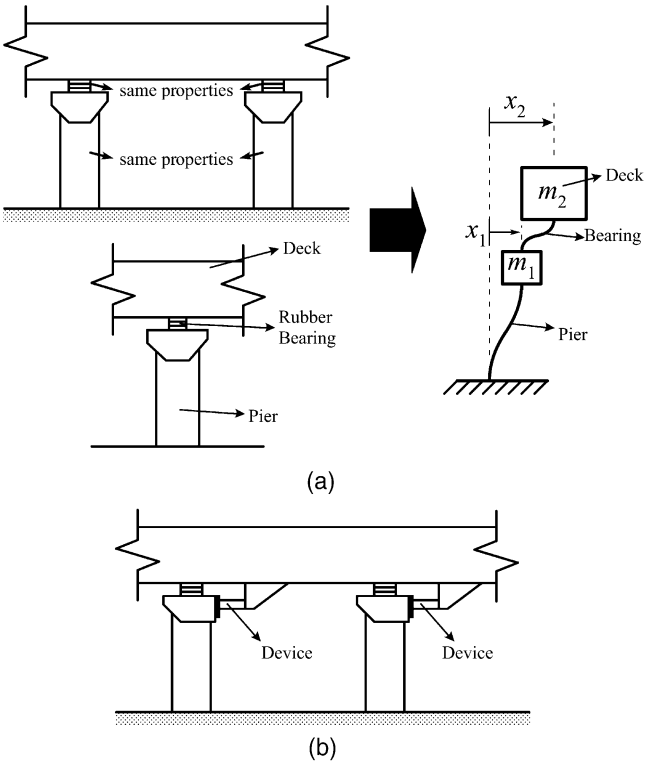

Fig. 1. Model of bridge: (a) two-DOF model; (b) placement of active and semi-active devices.

semi-active systems should be designed for optimal performances. However, design of these structures is not trivial owing to the dynamical characteristics of the bridge system: i.e., control forces that cannot be transferred to the ground but serve as internal force between deck and pier and unevenly distributed structural masses. Research on optimal design of two-DOF systems, analogous to the bridge model for free vibration or different types of excitation, comprises quite large field of study since several types of structure can be modeled as a two-DOF system. See, for example, Fujino and Abé [5] for a number of analytical works on optimization. Similar analytical methods can be employed for the two-DOF bridge model but they lack practicality for the analysis of higher DOF systems. In this case, numerical evaluation of a performance criterion is more convenient for an initial design. This criterion is generally based on maximum deformations since they are the most important indicators for the performance of systems excited by near-field earthquakes. Another tool used frequently for the evaluation of performance is root mean square (RMS) response. For example, Skinner et al. [6] used RMS responses to find the peak responses of low-mass secondary systems. Later, Abé and Fujino [7] defined a normalized peak response quantity using a similar approach as an indication of peak responses and employed it for optimal design of bridge bearings of a two-DOF bridge model. Such an approach is quite useful for an initial optimization study since it does not require extensive analytical and numerical work.

This paper investigates the applicability of semi-active control of elevated highway bridges for seismic protection by comparing the performances of optimally designed two-DOF passive, active and semi-active bridge models. In the first part of the paper, the concept of normalized peak response is defined and used to optimize the passive system, where the passive device is assumed to be a high-damping rubber bearing with linear stiffness and damping. Full state feedback linear quadratic regulator (LQR) control strategy is used for the active system. The main design parameter, known as **Q** matrix, is determined first, defining it as a function of a single parameter and then optimizing this parameter using normalized peak responses. An MR damper is used as the semi-active device and clipped optimal control is utilized to simulate the optimal control force obtained by the LQR algorithm. A simple method, which is based on maximum optimal control force, maximum damper displacements and velocities obtained from deterministic earthquake analysis of the active system, is used to design the MR damper. Each of the control systems is designed for three cases: reduction of pier response, reduction of bearing response and finally reduction of both responses. These systems are tested using three sets of ground acceleration data, and performances are compared using a performance index based on the maximum drifts together with an uncontrolled system with a low-damping bearing. Tabular and graphical results are given for all analyses.

2. Concept of normalized peak response

Consider a linear n-DOF system excited by stationary Gaussian white noise of duration τ. Mean maximum responses can be expressed as

$$\bar{R}_\tau^i = p^i \sigma^i, \tag{1}$$

where $\bar{R}_\tau^i$ and σ^i are the mean maximum response and root mean square response of DOF i, and p^i is a peak factor, which can be defined in terms of spectral moments and duration τ [8]. Now consider an SDOF system that is excited by the same random signal. An expression similar to Eq. (1) can be given in terms of another factor and the mean maximum response of the SDOF system as

$$\bar{R}_\tau^i = \gamma^i \bar{R}_{\mathrm{NS}} \tag{2}$$

where $\bar{R}_{\mathrm{NS}}$ is the mean maximum response of the SDOF system. Expressing γ^i in terms of mean maximum responses and using Eq. (1), one obtains

$$\gamma^i = \frac{\bar{R}_\tau^i}{\bar{R}_{\mathrm{NS}}} = \frac{p^i \sigma^i}{p_{\mathrm{NS}} \sigma_{\mathrm{NS}}} = p_{\mathrm{r}}^i \sigma_{\mathrm{r}}^i, \tag{3}$$

where p_r^i and σ_r^i are the ratios of peak factors and RMS responses, respectively. In this form, γ^i represents a normalized quantity and hence is called a normalized peak response by Abé and Fujino [7]. Following this definition, SDOF system used above is called a normalization system in this paper.

Now consider a system to be normalized. It is useful to use a normalization system where the approximation $p_r^i \approx 1$ can be used, which reduces Eq. (3) to

$$\gamma^i = \sigma_r^i. \tag{4}$$

Such an approximation is not always valid since p_r^i is a function of peak factors of both of the systems. It has been shown by Der Kiureghian [9] that the ratio of peak factors of a classically damped system to peak factors of its modal responses is around unity. This statement is not valid if the frequency of the highest mode is considerably small and the ratios of the modal frequencies are considerably large, which is not the case for most of the engineering structures modeled as finite-DOF systems. Comparing the modal combination rules for maximum responses of classically [9] and nonclassically [10] damped systems, one can easily show that this ratio is also around unity for nonclassically damped systems, which is also stated by Igusa and Der Kiureghian [10]. Hence, p_r^i of a classically or nonclassically damped system, which is normalized by an SDOF system, can take the values of possible ratios of peak factors of an SDOF system with damping ratio ξ_{NS} and natural frequency ω_{NS}, where ξ_{NS} and ω_{NS} are some acceptable values. Fig. 2 shows the change in maximum values of p_r^i with respect to ξ_{NS} for a set of mean zero crossings. Frequency values are also given for an earthquake duration of 100 s. As can be seen from this plot, this ratio may reach a value of 1.8 for some cases. Hence to use the approximation, an arbitrary normalization system cannot be chosen, but it should satisfy the following condition:

$$1-\varepsilon < p_r^i\{\xi_{NS}, \omega_{NS}\} < 1+\varepsilon, \tag{5}$$

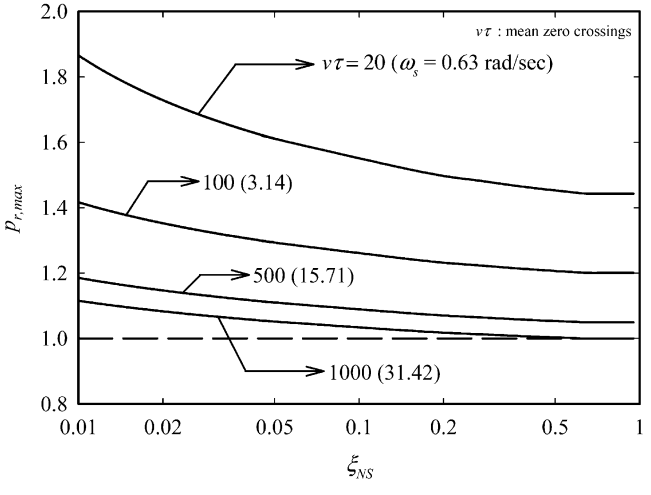

Fig. 2. Maximum peak factor ratios of an SDOF system.

where ε is an acceptable error. An SDOF system having a natural frequency between the highest and lowest modal frequencies of the original system will satisfy this condition with a slightly large value of ε, but will give reasonable results if the main purpose is to observe the change of the maximum response and not to obtain it numerically. In the latter case, an SDOF system that satisfies condition (5) for a smaller ε should be chosen. If $p_r^i \approx 1$ can be used, the final form of maximum responses will be

$$\bar{R}_\tau^i = \sigma_r^i \bar{R}_{NS}. \tag{6}$$

This equation is in the form used by Skinner et al. [6]. The merit of Eq. (6) is the fact that the peak factor and RMS value of an SDOF normalization system are easy to compute for random excitation. In the following sections of the study, γ^i and σ_r^i are used for optimization of the passive and active systems, which may be considered as examples of application of the method.

2.1. Computation of RMS of responses

Consider a system that is represented in its state space form as follows:

$$\dot{\mathbf{z}} = \mathbf{A}\mathbf{z} + \mathbf{B}\mathbf{u}, \tag{7}$$

where $\mathbf{z}$ is the state vector, $\mathbf{A}$ and $\mathbf{B}$ are the system matrices, $\mathbf{u}$ is the external excitation vector and the dot represents time derivation. Covariance matrix of $\mathbf{z}$ satisfies the following differential equation:

$$\dot{\mathbf{S}}_z = \mathbf{A}\mathbf{S}_z + \mathbf{S}_z\mathbf{A}^T + \mathbf{B}\mathbf{Q}(t)\mathbf{B}^T, \tag{8}$$

where $\mathbf{S}_z = E[\mathbf{z}\mathbf{z}^T]$ and is the covariance matrix of $\mathbf{z}$, and $\mathbf{Q}(t)$ is the covariance matrix of $\mathbf{u}$. If $\mathbf{u}$ is a stationary Gaussian white noise with zero mean and if its spectral density $\mathbf{G}(\omega) = \mathbf{G}_0$, $\mathbf{Q}(t)$ becomes a constant diagonal matrix and Eq. (8) reduces to following Lyapunov equation:

$$\mathbf{0} = \mathbf{A}\mathbf{S}_z + \mathbf{S}_z\mathbf{A}^T + \mathbf{B}\mathbf{Q}\mathbf{B}^T. \tag{9}$$

If the Fourier transform of a continuous function $f(t)$ is defined as

$$F(\omega) = \int_{-\infty}^{\infty} f(t)\, e^{-i\omega t}\, dt, \tag{10}$$

the diagonals of $\mathbf{Q}$ are equal to $\mathbf{G}_0$. Diagonal terms of $\mathbf{S}_z$ are mean square values of the state vector and solution of the equation can be used to estimate the RMS values. RMS values of specific quantities other than state variables can be found if these quantities can be expressed as a linear combination of the state vector as

$$\mathbf{y} = \mathbf{H}\mathbf{z}. \tag{11}$$

The covariance matrix of $\mathbf{y}$ can be found as

$$\mathbf{S}_y = E[\mathbf{y}\mathbf{y}^T] = \mathbf{H}\mathbf{S}_z\mathbf{H}^T, \tag{12}$$

where the diagonal terms of $\mathbf{S}_y$ are mean square values of $\mathbf{y}$.

3. Two-DOF modeling of the bridge and performance criterion

The bridge structures shown in Fig. 1 are modeled as a two-DOF system. The general form of the equation of motion for this system with or without a control device is

$$\mathbf{M}\ddot{\mathbf{x}} + \mathbf{C}\dot{\mathbf{x}} + \mathbf{K}\mathbf{x} + \mathbf{s}F_c = -\mathbf{M}\mathbf{r}\ddot{x}_g, \tag{13}$$

where $\mathbf{M}$ is the mass matrix; $\mathbf{C}$ is the damping matrix; $\mathbf{K}$ is the stiffness matrix; $\mathbf{s}$ is the location vector for control force, F_c; $\mathbf{x}$ is the displacement vector; $\mathbf{r}$ is the influence vector; and $\ddot{x}_g$ is the ground acceleration. The state space representation of the equation of motion can be written as

$$\dot{\mathbf{z}} = \mathbf{A}\mathbf{z} + \mathbf{B}F_c + \mathbf{G}\ddot{x}_g, \tag{14}$$

where $\mathbf{z}$ is the state vector and $\mathbf{A}$, $\mathbf{B}$ and $\mathbf{G}$ are the system matrices. If the control force is a constant gain linear feedback force such as

$$F_c = -\mathbf{K}_c\mathbf{z}, \tag{15}$$

where $\mathbf{K}_c$ is the gain matrix of dimensions 1×4, Eq. (14) reduces to

$$\dot{\mathbf{z}} = \tilde{\mathbf{A}}\mathbf{z} + \mathbf{G}\ddot{x}_g, \tag{16}$$

where

$$\tilde{\mathbf{A}} = \mathbf{A} - \mathbf{B}\mathbf{K}_c; \tag{17}$$

the state vector and the system matrices are

$$\mathbf{z} = \begin{bmatrix}\mathbf{x}\\ \mathbf{v}\end{bmatrix},\ \mathbf{A} = \begin{bmatrix}\mathbf{0} & \mathbf{I}\\ -\mathbf{M}^{-1}\mathbf{K} & -\mathbf{M}^{-1}\mathbf{C}\end{bmatrix}, \tag{18}$$

$$\mathbf{B} = \begin{bmatrix}\mathbf{0}\\ -\mathbf{M}^{-1}\mathbf{s}\end{bmatrix} \text{ and } \mathbf{G} = \begin{bmatrix}\mathbf{0}\\ -\mathbf{r}\end{bmatrix},$$

in which

$$\mathbf{M} = \begin{bmatrix}m_1 & 0\\ 0 & m_2\end{bmatrix},\ \mathbf{C} = \begin{bmatrix}c_1+c_2 & -c_2\\ -c_2 & c_2\end{bmatrix},$$

$$\mathbf{K} = \begin{bmatrix}k_1+k_2 & -k_2\\ -k_2 & k_2\end{bmatrix},\ \mathbf{s} = \begin{bmatrix}-1\\ 1\end{bmatrix},\ \mathbf{r} = \begin{bmatrix}1\\ 1\end{bmatrix}, \tag{19}$$

$$\mathbf{x} = \begin{bmatrix}x_1\\ x_2\end{bmatrix} \text{ and } \mathbf{v} = \dot{\mathbf{x}}.$$

In the above, m_1 and m_2 are the lumped masses of the pier and deck, respectively; c_1 and c_2 are the damping constants of the pier and bearing, respectively; k_1 and k_2 are the stiffness constants of the pier and bearing, respectively; and x_1 and x_2 are the pier and deck displacements relative to the ground, respectively. In passive control, F_c is taken as zero.

For simulation purposes, mass ratio, damping ratio and the natural period of the pier are set to $\mu(=m_2/m_1)$=5, 5% and 0.5 s, respectively, which are typical values for elevated highway bridges. Then, k_1 and c_1 are calculated representing the pier as an SDOF system with mass m_1, stiffness k_1 and damping constant c_1. The damping ratio and natural frequency of the corresponding system are designated as ξ_1 and ω_{pier}. Similarly, the natural period and the damping ratio of the bearing are calculated considering an SDOF system with parameters m_2, k_2 and c_2, and the corresponding damping ratio ξ_2 and natural frequency ω_{bearing} are found. In the numerical simulations, the mass of the pier is taken as 100 tons and other parameters are calculated accordingly.

To compare the efficiency of the control strategies, a performance criterion is defined based on the maximum drifts as follows:

$$J = [\{ax_1^{\max}\}^2 + \{b(x_2 - x_1)^{\max}\}^2]^{1/2}. \tag{20}$$

The parameters a and b are defined according to the relative performances of the pier and deck. In this study, three design goals are studied; based on these goals, three sets of parameters are defined as in Table 1.

4. Passive system

In this section, first normalized displacements are used to optimize the passive system. Two types of normalization system are considered and random vibration analysis results are compared with earthquake analyses. The first system is an SDOF and the second is a classically damped two-DOF system. Then, according to the results obtained, three passive systems are designed for three design goals.

4.1. SDOF case

The SDOF system used by Abé and Fujino [7] is used as the first normalization system where SDOF represents the bridge system when the deck is not isolated but fixed. Hence γ^j represents the reduction ratio of response by the passive device. RMS of an SDOF system under Gaussian white noise ground acceleration with zero

Table 1
Performance index parameters

Design	Main design goal	a	b
D1	Minimize pier response	1	0
D2	Minimize bearing response	0	1
D3	Minimize both pier and bearing responses	1	1

mean and spectral density G_0 can be found easily using Eq. (9) as

$$\sigma_{NS}=\frac{G_0}{4\xi_{NS}\omega_{NS}^3}. \tag{21}$$

4.2. Two-DOF case

Instead of the SDOF system given in the previous section, a two-DOF or another SDOF system can be designed so that Eq. (5) is valid for a smaller value of ε. In this section a two-DOF system is studied, which makes the SDOF case straightforward. Final normalized displacements become

$$\gamma^1=\frac{\bar{R}_\tau^1}{\bar{R}_{NS}^1}=\frac{p^1\sigma^1}{p_{NS}^1\sigma_{NS}^1}=p_r^1\sigma_r^1 \text{ and } \gamma^2=\frac{\bar{R}_\tau^2}{\bar{R}_{NS}^2}=\frac{p^2\sigma^2}{p_{NS}^2\sigma_{NS}^2} \tag{22}$$
$$=p_r^2\sigma_r^2.$$

Mass and stiffness matrices of the normalization system are taken to be the same as for the original system but the damping is assumed to be Rayleigh damping. The bearing is assumed to have an optimal stiffness found for a similar two-DOF system by Fujino and Abé [5], and is estimated by the relation

$$\frac{\omega_{bearing}}{\omega_{pier}}=\frac{\sqrt{1+(\mu/2)}}{1+\mu}. \tag{23}$$

Modal damping ratios of the normalization system are investigated so that $p_r^i\approx 1$ can be used. Peak factors can be found by dividing maximum responses by RMS values. In this case, maximum values can be calculated by use of the combination rule given by Der Kiureghian [9]. A similar combination rule or Lyapunov equation can be used to find RMS responses. Average ratios of the peak factors of the normalization system to itself are investigated over a range (0.01, 0.50) of modal damping ratios of the normalization system, so that averages are in between (1.0005, 0.9995). Fig. 3 shows the values of the modal damping ratios where the above conditions are satisfied for the peak factor ratios of both DOFs. Hence a two-DOF normalization system with modal damping ratios of 0.18 for the first mode and 0.13 for the second mode are used for the analysis. Although the main design parameters are stiffness and the damping of the bearing, in this section stiffness is fixed to Eq. (23) to enable easy comparison of the results with the earthquake analysis.

Normalized displacements, γ^j, are obtained for two normalizations systems under Gaussian white noise for a set of damping ratios of the bearing. These normalized displacements are designated as γ_{RV}^j. Two sets of γ^j are calculated for three earthquakes: El Centro, Northridge and Kobe. One set is found using the RMS values and the other set is found using maximum responses. They are designated as γ_{RMS}^j and γ_{MAX}^j, respectively. Then, they are compared with γ_{RV}^j through figures. In Fig. 4, the normalized displacements are found using RMS values for both earthquakes and the random signal. In Fig. 5 these values are found using maximum values for earthquakes and RMS values for the random signal. The efficiency of Eq. (6) is investigated by comparing the maximum displacements obtained from this equation with the actual maximum values obtained from earthquake analysis as in Fig. 6.

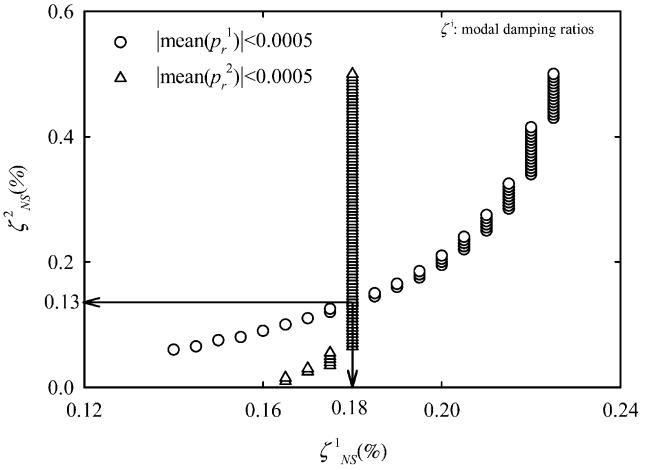

Fig. 3. Determination of modal damping ratios for |mean(p_r)|< 0.0005.

From these figures strict generalizations cannot be extracted but it can be easily observed that γ_{RV}^j shows the trends of γ_{RMS}^j and γ_{MAX}^j for both of the normalization systems, while the two-DOF normalization system can predict γ_{RMS}^j better. Hence, γ_{RV}^j can be used for optimization purposes since the characteristics of the normalization system used herein are constants. Also it is observed that with this form, maximum responses found by random vibration analysis and normalized displacements cannot predict actual maximum responses efficiently. This is mainly due to the constant characteristics of the normalization system.

The most important observation related to the performance of the bridge is that pier responses do not decrease continually with the increase in bearing damping. This is more apparent for the Kobe and Northridge earthquakes. Both maximum and normalized maximum displacements give minimum pier responses for $0.3<\xi_2<0.5$. Also it is observed that bearing drifts decrease with the increase in bearing damping.

Numerical simulations up to this point are carried out basically for investigation of the validity of the concept of normalized displacements fixing bearing stiffness. However, for a full optimization, the stiffness of the bearing should also be investigated. Such a study was done by Abé et al. [11], and shows that a continuous

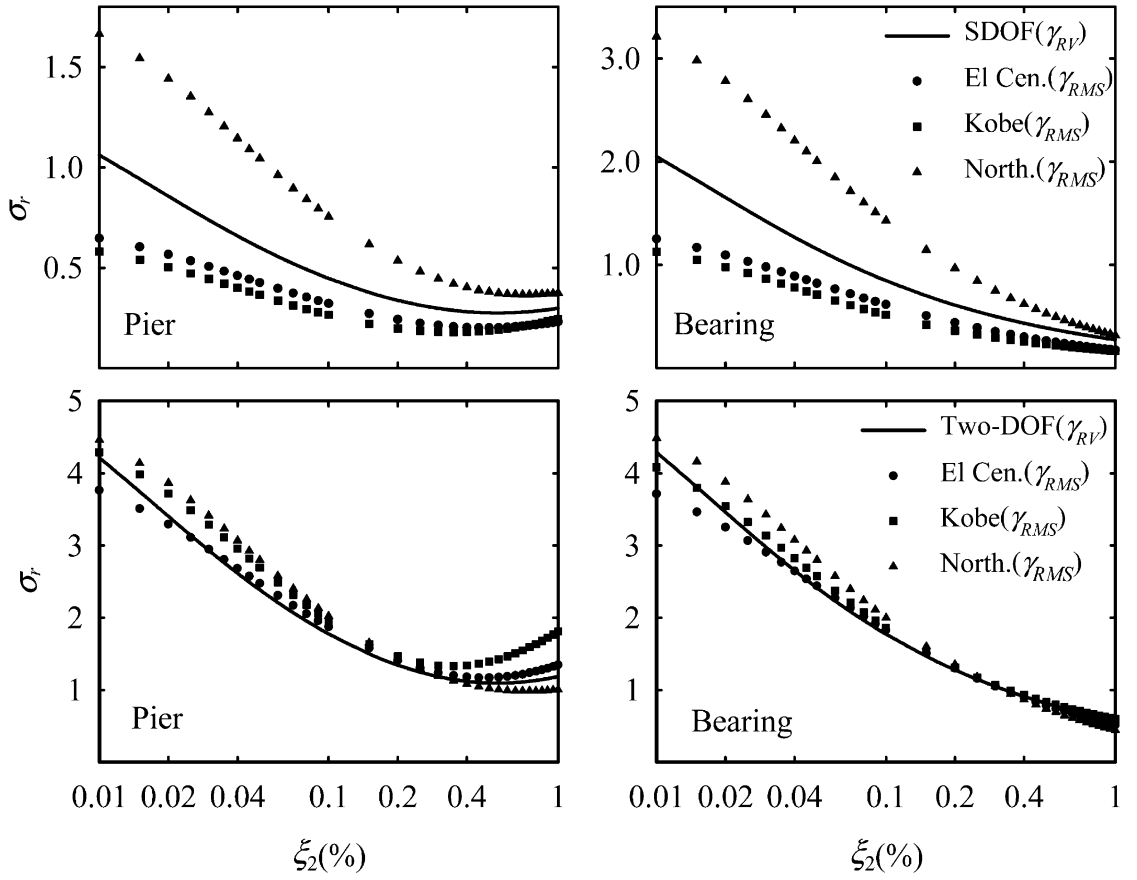

Fig. 4. Normalized peak responses when RMS values are used.

increase in bearing stiffness causes a continuous increase in pier response but a continuous decrease in bearing response. Hence, different stiffnesses should be used for different design goals, which makes the problem more complex. Instead, the same stiffness obtained from Eq. (23) is used for the three designs and three control strategies in this study. Final damping ratios of the bearing are chosen as 0.4, 1.0 and 0.7 for designs D1, D2 and D3, respectively.

5. Active system

The LQR control strategy is used for active and semi-active control. The LQR problem is defined as the minimization of a quadratic objective function given by

$$J=\int_0^T (\mathbf{z}^T\mathbf{Q}\mathbf{z}+\mathbf{u}^T\mathbf{R}\mathbf{u})\,dt \tag{24}$$

with respect to **u**, subjected to the state equation of a system given by

$$\dot{\mathbf{z}}=\mathbf{A}\mathbf{z}+\mathbf{B}\mathbf{u}+\mathbf{f}, \tag{25}$$

where **z** is a $2n\times1$ state vector, **u** is a $k\times1$ control force vector, **f** is the external disturbance vector, **A** is a $2n\times2n$ system matrix, **B** is a $2n\times k$ matrix defining the location of control force. **Q** and **R** are $2n\times2n$ and $k\times k$ positive definite weight matrices and are determined according to the design goal and constraints on control forces. Assuming that $E[\mathbf{f}]=\mathbf{0}$, minimization of Eq. (24) under Eq. (25) when $T\rightarrow\infty$ gives the control force as

$$\mathbf{u}=-\mathbf{R}^{-1}\mathbf{B}^T\mathbf{P}\mathbf{z}, \tag{26}$$

where **P** is the solution of the well-known Ricatti equation given by

$$\mathbf{A}^T\mathbf{P}+\mathbf{P}\mathbf{A}+\mathbf{Q}-\mathbf{P}\mathbf{B}\mathbf{R}^{-1}\mathbf{B}^T\mathbf{P}=\mathbf{0}. \tag{27}$$

Q and **R** are the main design parameters of the active controller and extensive study should be carried out to determine the values of these parameters for better performance of the active system, which is beyond the scope of this study. Here, **Q** matrix is represented by a parameter *r*, based on the energy of the SDOF systems of mass m_1 and m_2 defined before such that

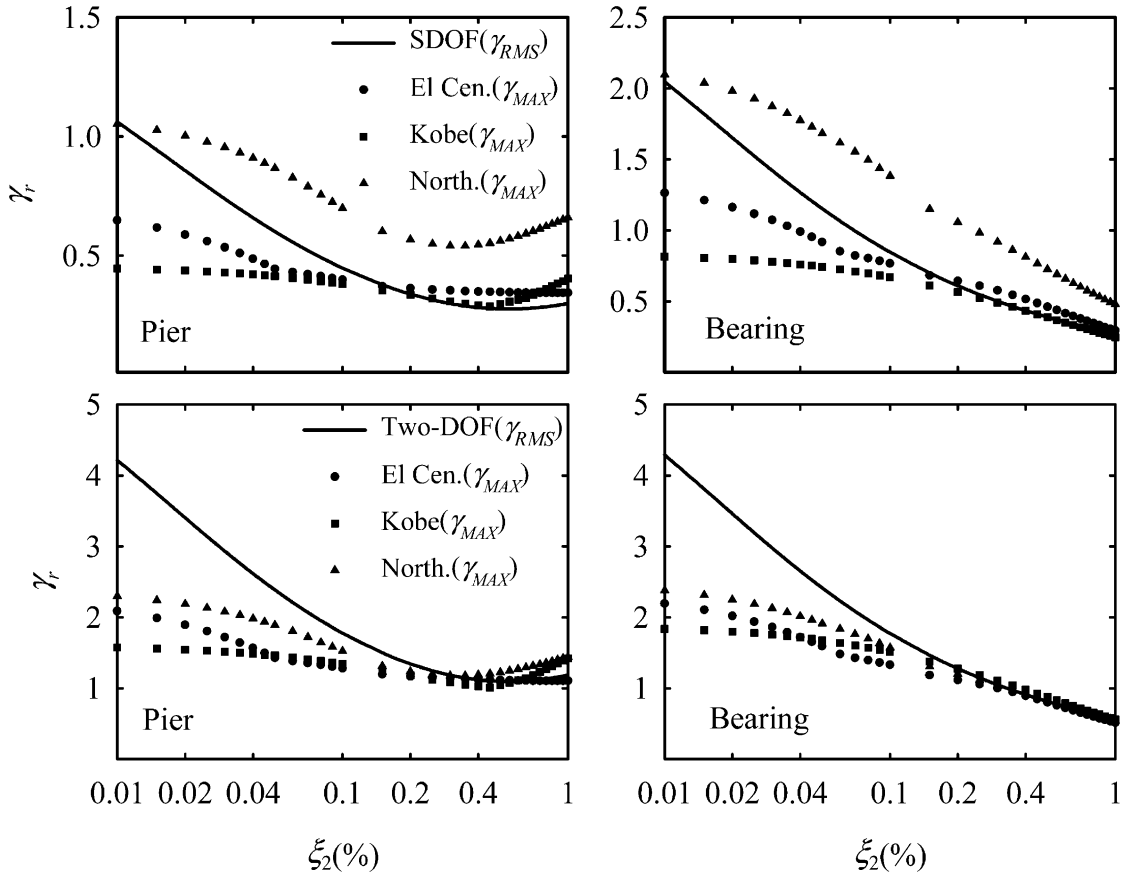

Fig. 5. Normalized peak responses when maximum values for earthquakes are used.

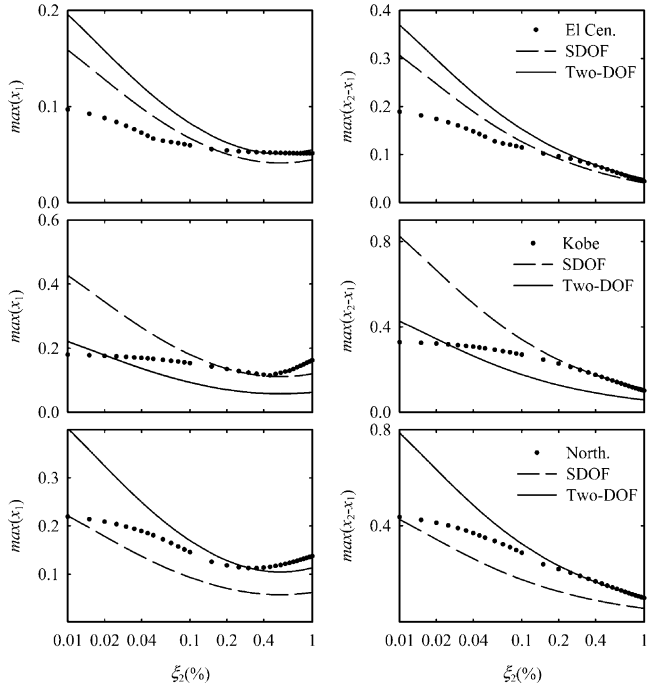

Fig. 6. Comparison of maximum responses.

$$\mathbf{z}^{\mathrm{T}}\mathbf{Q}\mathbf{z}=r\left\{\frac{1}{2}k_1(x_1)^2+\frac{1}{2}m_1(v_1)^2\right\}+\left\{\frac{1}{2}k_2(x_2-x_1)^2+\frac{1}{2}m_2(v_2-v_1)^2\right\}. \tag{28}$$

In this equation, the term in the first bracket represents the energy of the pier and that in the second bracket represents the energy of the deck and bearing; parameter r defines the relative importance of pier and bearing responses. A larger value of r is expected to decrease the pier response and vice versa. Eq. (28) yields $\mathbf{Q}$ as

$$\mathbf{Q}(r)=\begin{bmatrix}\frac{1}{2}(rk_1+k_2) & -\frac{1}{2}(k_2) & 0 & 0\\ -\frac{1}{2}(k_2) & \frac{1}{2}(k_2) & 0 & 0\\ 0 & 0 & \frac{1}{2}(rm_1+m_2) & -\frac{1}{2}(m_2)\\ 0 & 0 & -\frac{1}{2}(m_2) & \frac{1}{2}(m_2)\end{bmatrix}. \tag{29}$$

It is assumed that $\mathbf{R}$ can take any value, hence active

control design reduces to the problem of determination of parameter r for the three design goals.

The effect of r on the normalized displacements, which are computed using the two-DOF normalization system obtained in the previous sections, is shown in Fig. 7. **R** is taken as 1×10^{-12} after some trial runs and normalized displacements are obtained using a two-DOF normalization system. Also, the normalized displacements for three earthquakes are given. As can be seen from this plot, normalized displacements obtained from random vibration analyses can predict the trend in behavior very well and hence can be used for optimization. The differences between the EQ and random responses may be attributed to the normalized system, which was chosen for the passive system but not for the active system. Finally, three r values are chosen as 1000, 0.1 and 10 for designs D1, D2 and D3, respectively.

6. Semi-active control

In this section, the MR damper is chosen as semi-active device and the voltage of the device is commanded by the clipped optimal control strategy proposed by Dyke et al. [1] to simulate the control force obtained from the LQR control strategy. The equation of motion of the system is same as Eq. (13) except that F_c is replaced by F_d, where F_d is damper force. According to clipped optimal control, the voltage applied to the MR damper changes as follows:

$$v^t=v_{\max}H(\{F_c^t-F_d^{t-1}\}F_d^{t-1}), \tag{30}$$

where v^t is the voltage applied at time t, $v_{\max}$ is the maximum voltage that can be applied to the MR damper, F_c^t and F_d^{t-1} are the optimal control force and damper force at time t and $t-1$, respectively and $H(\cdot)$ is the Heaviside step function. Optimal control force is obtained with Eq. (26) using the state vector obtained during semi-active simulation.

The MR damper model proposed by Spencer et al. [12], which is based on the Bouc–Wen model, is used (Fig. 8). The governing equations of the model are

$$F_d=\alpha z+c_0(\dot{x}-\dot{y})+k_0(x-y)+k_1(x-x_0), \tag{31}$$

$$\dot{z}=-\gamma|\dot{x}-\dot{y}||z|z|^{n-1}-\beta(\dot{x}-\dot{y})|z|^n+A(\dot{x}-\dot{y}), \tag{32}$$

$$\alpha=\alpha_a+\alpha_b u, \tag{33a}$$

$$c_1=c_{1a}+c_{1b}u, \tag{33b}$$

$$c_0=c_{0a}+c_{0b}u \tag{33c}$$

and

$$\dot{u}=-\eta(u-v), \tag{34}$$

where x is the displacement of the damper, F_d is the force generated by the damper and v is the voltage applied to the damper. Other parameters will be given later.

The model defined above is based on a prototype model of the MR damper, which cannot be used in real structures. One way to incorporate this model into the two-DOF bridge system is to modify the parameters of the MR damper, multiplying the damping, stiffness and hysteretic constants of the model by a modification factor, MF, to magnify the damper force. Practically this is same as using MF dampers. However, this factor is not arbitrary and should be determined so that the system behaves optimally. Normalized peak displacements can be used to find the optimal MFs. To find the mean square responses, equivalent linearization techniques [13,14] should be used to represent the damper model in the state space analysis. In this paper MF is determined using a simple method based on the deterministic analysis of the active system instead of random vibration analysis of the semi-active system. This method can be summarized as follows.

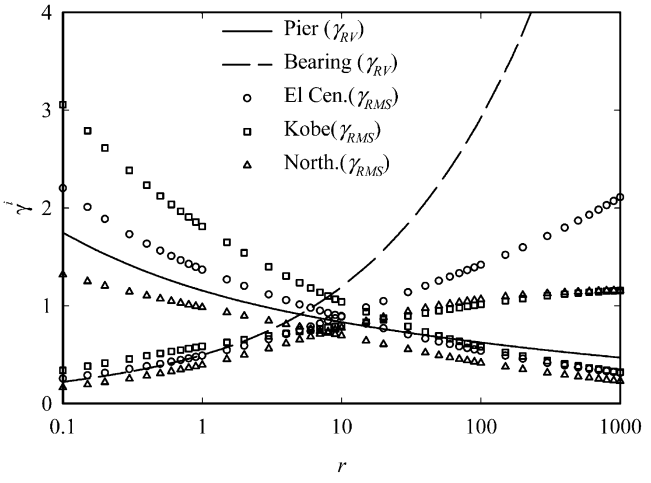

Fig. 7. Normalized peak responses of active system.

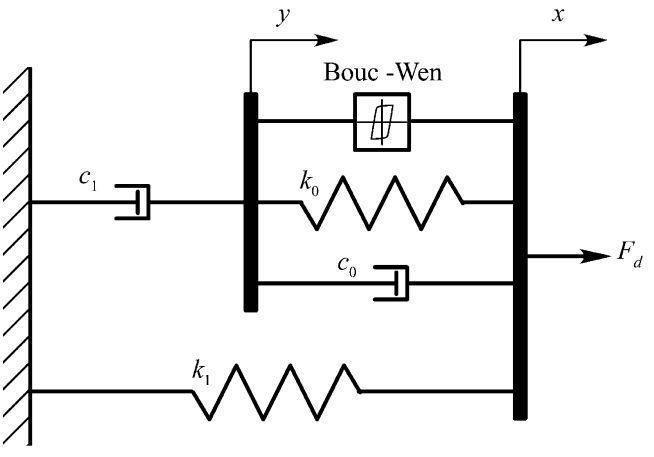

Fig. 8. Model of MR damper (Spencer et al. [12]).

Table 2
Design values of MF

		$(x_2-x_1)^{max}_{act}$ (cm)	$(v_2-v_1)^{max}_{act}$(cm/s)	F_c^{max} (kN)	ω (rad/s)	F_d^{max} (kN)	MF	Average MF
D1	El Centro	12.65	33.94	845.8	2.68	2.24	377.7	394.8
	Kobe	20.87	87.84	1404.9	4.21	3.74	375.8	
	Northridge	24.04	80.51	1560.5	3.35	3.62	430.9	
D2	El Centro	1.94	10.30	1089.9	5.31	1.45	750.6	1264.0
	Kobe	5.65	35.13	3611.5	6.22	2.15	1681.2	
	Northridge	4.16	18.18	2291.7	4.37	1.68	1360.3	
D3	El Centro	7.06	26.57	570.3	3.76	1.94	293.2	410.3
	Kobe	12.97	85.55	1610.4	6.60	3.56	452.7	
	Northridge	16.5	71.90	1580.3	4.36	3.26	485.0	

1. Find the maximum optimal control force, maximum bearing displacement and maximum bearing velocity of the active system; i.e., F_c^{max}, $(x_2-x_1)^{max}_{act}$ and $(v_2-v_1)^{max}_{act}$.
2. Apply a sinusoidal excitation with amplitude and frequency given by

$$x_0=(x_2-x_1)^{max}_{act} \tag{35}$$

and

$$\omega_d=\frac{(v_2-v_1)^{max}_{act}}{(x_2-x_1)^{max}_{act}}, \tag{36}$$

respectively, to the original damper model and find the maximum damper force, F_d^{max}.
3. MF is given by

$$MF=\frac{F_c^{max}}{F_d^{max}}. \tag{37}$$

Table 2 gives the tabular results of the method for the three designs. Average values of MF for the three earthquakes are used to find the final MF. The final form of damper parameters is given in Table 3.

Table 3
Modified MR damper parameters

Parameter	Value
c_{0a} (N s/cm)	21MF
c_{0b} (N s/cm)	3.5MF
k_0 (N/cm)	46.9MF
c_{1a} (N s/cm)	283MF
c_{1b} (N s/cm V)	2.95MF
k_1 (N/cm)	5.0MF
x_0 (cm)	14.3
α_a (N/cm)	140MF
α_b (N/cm V)	695MF
γ (cm^{-2})	363
β (cm^{-2})	363
A	301
n	2
η (s^{-1})	190

7. Numerical simulations and discussion of results

The performances of the controlled systems are compared using ground motion data from three earthquakes: El Centro, Kobe and Northridge. Also, an uncontrolled system with a low-damping bearing is analyzed for comparison purposes. Characteristics of the systems are summarized in Table 4.

Tables 5 and 6 give the tabular results of performance indices, where lower values show an increased performance. Fig. 9 shows the simulation results for the three designs. As can be seen from the figure and tables, fully active control decreases the pier responses considerably in the first design while it increases the deck responses. The semi-active system cannot simulate active behavior and shows a similar response to the passive system. In the second design, where the goal is reduce the bearing response, the active and semi-active systems show better performance. In fact, their response histories are almost identical, which means that the semi-active system can mimic the active system efficiently. However, the decrease in bearing responses cause a considerable increase in the pier responses. The main reason for the increased responses of the pier is the transfer of control force to the other mass but not to a fixed point such as ground. The response histories of the systems, where the

Table 4
Summary of the systems compared

	Uncontrolled c_2 (kN s/m)	Passive c_2 (kN s/m)	Active r	Semi-active MF
D1	196.0	1468	1000	394.8
D2		3920	0.1	1264.0
D3		2744	10	410.3
m_1 (tons)			100	
m_2 (tons)			500	
k_1 (kN/m)			15,791	
k_2 (kN/m)			7685	
c_1 (kN s/m)			125.6	
c_2 (kN s/m)			0	0

Table 5
Performance indices of the controlled systems

	D1 (cm)				D2 (cm)				D3 (cm)			
	Uncontrolled	Passive	Active	Semi-active	Uncontrolled	Passive	Active	Semi-active	Uncontrolled	Passive	Active	Semi-active
El Centro	6.64	5.22	**1.21**	4.97	13.75	4.40	1.94	**1.90**	15.28	**7.63**	8.10	7.81
Northridge	16.7	11.89	**3.29**	15.69	29.91	9.95	**5.65**	6.04	34.25	18.60	**16.51**	21.20
Kobe	18.03	11.30	**3.14**	12.11	34.89	9.95	4.16	**3.99**	39.27	**17.71**	18.73	18.70

Table 6
Percentage reduction in the performance indices with respect to the uncontrolled system

	D1 (%)			D2 (%)			D3 (%)		
	Passive	Active	Semi-active	Passive	Active	Semi-active	Passive	Active	Semi-active
El Centro	21	**82**	25	68	**86**	86	**50**	47	49
Northridge	29	**80**	6	67	**81**	80	46	**52**	38
Kobe	37	**83**	33	71	88	**89**	**55**	52	52

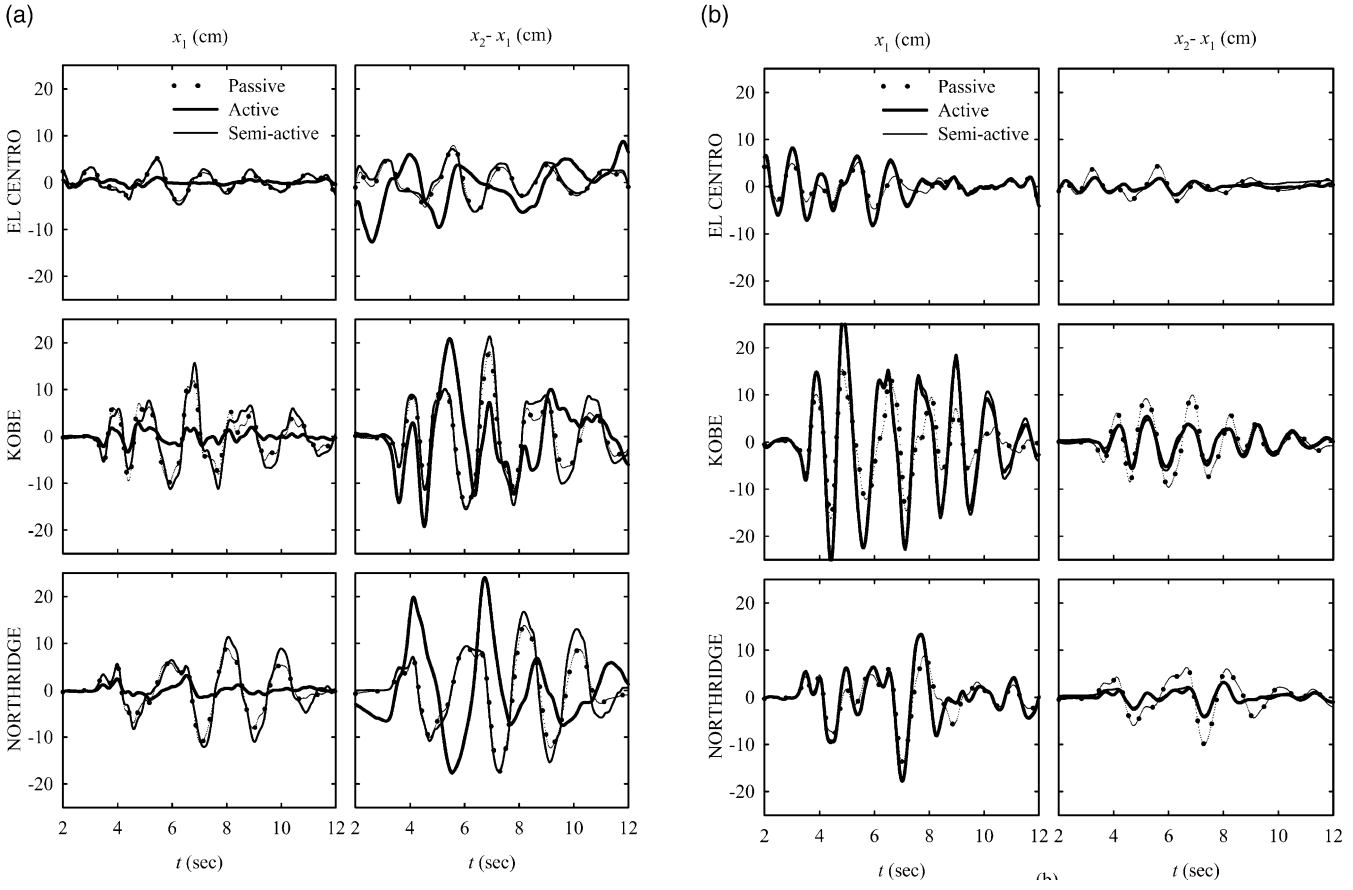

Fig. 9. Response–time histories of (a) D1, (b) D2 and (c) D3.

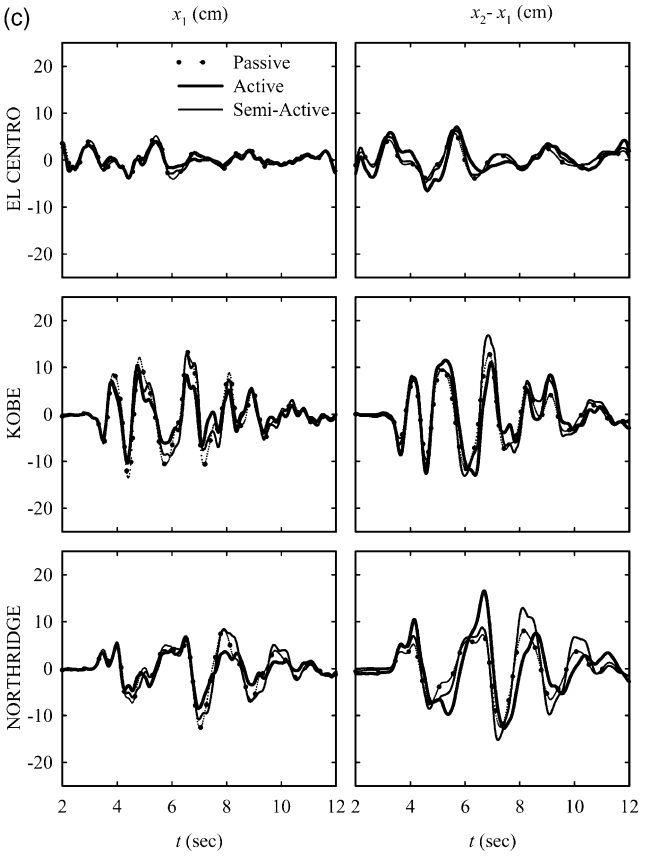

Fig. 9. (*continued*)

design goal is to reduce both drifts, are almost same. In this case the semi-active system mimics the active system but not efficiently as in the second design. Hence, the active control design should be improved for better performance of the semi-active system for this design.

In addition to response histories, comparison of the optimal control forces and damper forces will aid in understanding the behavior. Fig. 10 shows the damper and optimal control forces. Relations between the optimal control force, damper velocity and displacement are also presented. In the first design, the damper cannot simulate the optimal control force and the damper velocities do not occur in the direction of the optimal control force, rather they are arbitrary. Also the damper displacements do not show a pattern. However, this is not the case in the second design. Damper forces can simulate the active control force efficiently. The velocities occur in the direction of the optimal control force and the relation between optimal control forces and damper displacements shows an elliptic pattern, which means that the damper dissipates energy like a linear viscous damping. Another observation is that huge damper forces occur in the Kobe simulations, although this is not the case for the other earthquakes: for example, the damper forces are same as control forces for the Northridge earthquake. Hence the MR damper design is well-suited for this latter earthquake but not for Kobe. Also, although the maximum damper forces are very large, the damper is able to simulate the control force, which means that over-design of damper does not affect the damper performance. In the third design, these relations are similar to the second design but they are somewhat distorted. Also, it is observed that the control forces needed in the first and third design are lower than the forces in the second design since the second design aims to decrease drift associated with the damper and bearing.

The above observations can also be explained using modal responses. In a two-DOF bridge system, the first mode dominates the responses. Now consider the control forces needed for the first and second designs. The directions of these forces are shown in Fig. 11. Also shown in this figure is the direction of forces that can be produced by the damper in this mode. As can be seen, the damper is effective in the second design due to the control force direction. Hence, it may be beneficial to analyze how the damper force direction changes for several values of r. For this purpose an index that shows the percentage occurrence of v_2-v_1 in the direction of control force is found during the active control simulation. Although v_2-v_1 does not show the damper force direction exactly, it can be used as an indicator. Fig. 7 is regenerated showing this index and Fig. 12 is obtained. In this figure, instead of the normalized active response itself, the percentage increase in the normalized active response with respect to the normalized passive response is shown. The passive system used in these calculations is chosen to be the system used in D3. As can be seen, for higher values of r, v_2-v_1 occurs less in the direction of the control force. This may be an indication of the effectiveness of the damper. Hence the shaded area shows the region where the semi-active device is expected to be more effective than the passive system.

8. Conclusions

Semi-active control is investigated for seismic protection of elevated highway bridges. An MR damper with LQR-based clipped optimal control is used in semi-active control and its performance is compared with that of optimally designed passive and active systems for three design goals. The following conclusions can be drawn.

1. In passive control, a continuous increase in the damping of the bearing causes a continuous decrease in the responses of both pier and deck until the damping reaches a specific value. After this value, the pier response increases while the deck response continues to decrease.
2. Optimally designed active systems decrease the pier

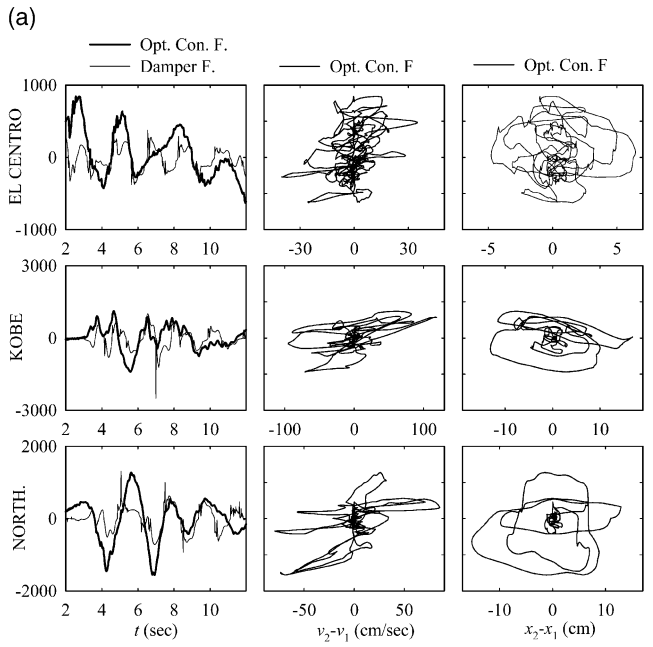

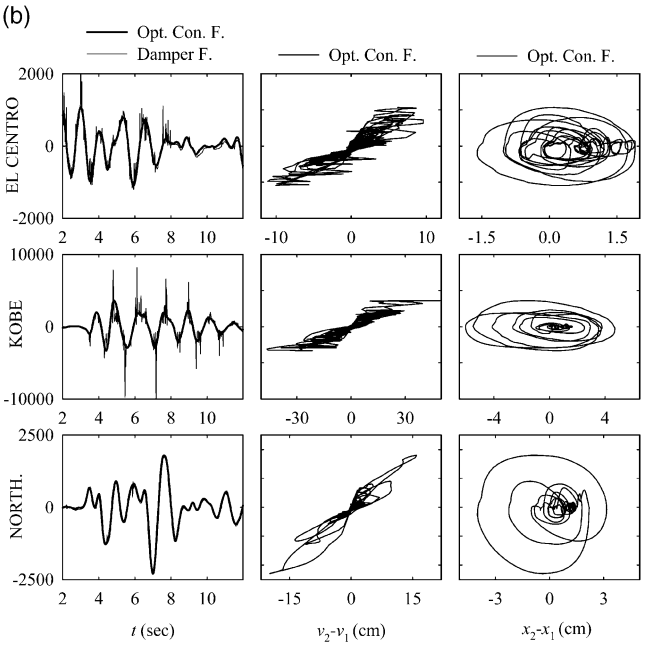

Fig. 10. Comparison of optimal control forces of active simulation and damper forces, damper velocities and damper displacements of semi-active simulation: (a) D1; (b) D2; (c) D3.

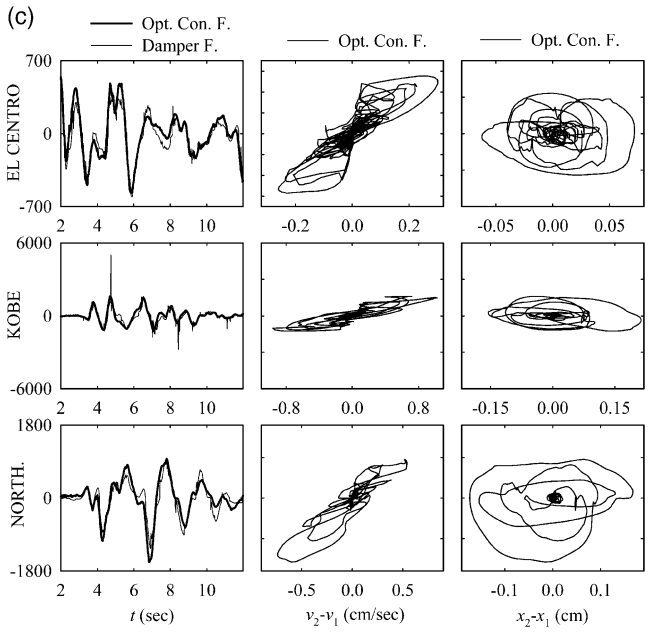

Fig. 10. (*continued*)

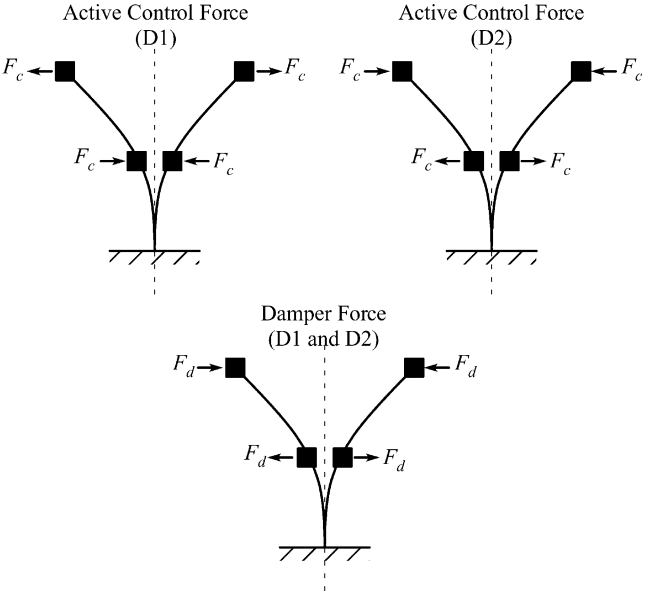

Fig. 11. Direction of control forces and damper forces in the first mode.

response or the deck response considerably. However, the system designed to decrease both responses does not show better performance than the passive system. Hence, a separate study should be carried out to obtain better active performance for this design goal.

3. The semi-active system shows similar performance to the passive system when the design goal is to reduce pier response. When the design goal is to reduce deck responses, it reaches the active system performance, and has almost the same time–response history as the active system. It shows similar performance to the active system in the third design, where the aim is to reduce both responses, but does not improve the passive system since the active system does not cause improvement. These results are devoted to semi-active characteristics of the MR damper.

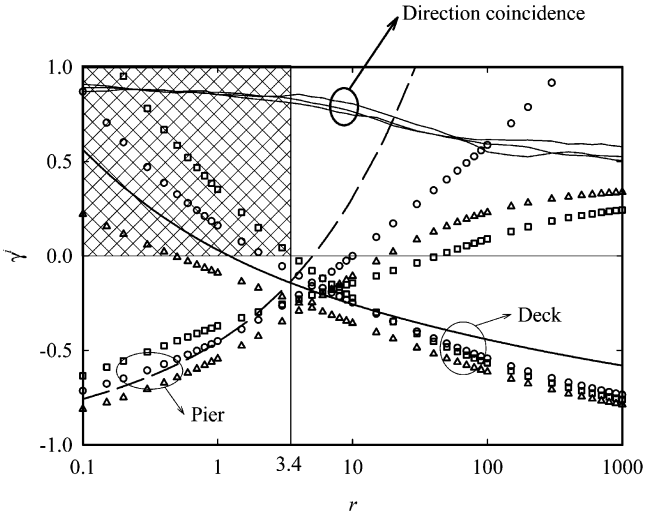

Fig. 12. Percentage increase in the active normalized responses and direction coincidence.

Acknowledgements

This research was supported by the Ministry of Education, Science, Sports and Culture of Japan. This support is gratefully acknowledged.

References

[1] Dyke SJ, Spencer BF Jr., Sain MK, Carlson JD. Modeling and control of magnetorheological dampers for seismic response reduction. Smart Mater Struct 1996;5:565–75.

[2] Dyke SJ, Spencer BF Jr., Sain MK, Carlson JD. An experimental study of MR dampers for seismic protection. Smart Mater Struct 1997;7:693–703 [special issue on Large Civil Structures].

[3] Kawashima K, Unjoh S. Seismic response control of bridges by variable dampers. J Struct Eng, ASCE 1994;120(9):2583–601.

[4] Symans MD, Kelly SW. Fuzzy logic control of bridge structures using intelligent semi-active seismic isolation systems. Earthquake Eng Struct Dyn 1999;28:37–60.

[5] Fujino Y, Abé M. Design formulas for tuned mass dampers based on a perturbation technique. Earthquake Eng Struct Dyn 1993;22:833–54.

[6] Skinner RI, Robinson WH, McVerry GH. In: An introduction to seismic isolation. Chichester, England: John Wiley and Sons, 1993:212–3.

[7] Abé M, Fujino Y. Optimal design of passive energy dissipation devices for seismic protection of bridges. J Struct Mech Earthquake Eng, JSCE 1998;605(I-45):241–52 (in Japanese).

[8] Der Kiureghian A. Structural response to stationary excitation. J Eng Mech Div, ASCE 1980;106(EM6):1195–213.

[9] Der Kiureghian A. A response spectrum method for random vibration analysis of MDF systems. Earthquake Eng Struct Dyn 1981;9:419–35.

[10] Igusa T, Der Kiureghian A. Dynamic response of multiply supported secondary systems. J Eng Mech Div, ASCE 1985;111(1):20–41.

[11] Abe M, Erkus B, Fujino Y, Park K-S. Applicability of semi-active control for seismic protection of elevated bridges. In: 55th Annual Meeting of JSCE, Kyoto, Japan, September 21–23, 2000. CD-ROM Proceedings. Paper No: I-A163.

[12] Spencer BF Jr., Dyke SJ, Sain MK, Carlson JD. Phenomenological model for magnetorheological dampers. J Eng Mech, ASCE 1996;123(3):230–8.

[13] Baber AM, Wen Y-K. Random vibration of hysteretic, degrading systems. J Eng Mech, ASCE 1981;107(EM6):1069–87.

[14] Hurtado JE, Barbat AH. Equivalent linearization of Bouc–Wen hysteretic model. Eng Struct 2000;22:1121–32.